I-F Control With Zero D-Axis Current Operation for Surface-Mounted Permanent Magnet Synchronous Machine Drives

Dunzhi Chen, *Student Member, IEEE*, Kaiyuan Lu, *Member, IEEE*, Dong Wang, *Member, IEEE*, and Marko Hinkkanen, *Fellow, IEEE*

***Abstract*—This article deals with I-f control of surface-mounted permanent magnet synchronous machine (SPMSM) drives. Conventional open-loop I-f control is poorly damped and can only operate stably with positive d-axis current. An I-f control with a new current compensation loop is proposed to achieve stable $i_{\mathrm{d}} = 0$ operation in this work. The proposed method can be used for startup with a seamless transition to sensorless field-oriented-control (FOC), since $i_{\mathrm{d}} = 0$ operation is already achieved before switching to FOC. In addition, as the I-f control can now maintain stable $i_{\mathrm{d}} = 0$ operation against 100% rated load step disturbance from 10% to 100% rated speed, it could be a standalone control scheme for wide-speed-range operations. The proposed method is supported with detailed stability analysis and its performance is verified experimentally on a 2.7-kW SPMSM drive platform.**

***Index Terms*—Efficiency, i-f control, scalar control, sensorless control, stability, surface-mounted permanent magnet synchronous machine (SPMSM).**

I. Introduction

SENSORLESS control of permanent magnet synchronous machine (PMSM) drives is of great interest for cost reduction and reliability enhancement, and has been studied in detail over the past decades.

Back electromotive force (EMF)-based sensorless field-oriented-control (FOC) [1], [2], [3] is widely used in practical applications. However, these methods deteriorate in low speed and fail at standstill. Therefore, a startup strategy is usually needed before using them. Signal injection (SI)-based methods [4] can provide high-performance startup. For demanding applications, SI and back EMF-based methods should be combined for high performance in the whole speed range [5], [6]. However, when PMSMs are used for applications with moderate shaft dynamics, scalar (V/f and I-f) control is also popular due to their simplicity and ease of implementation. Two ways of using scalar control have been reported: as a startup method [7], [8], [9], [10], [11], [12], [13], [14] and as a standalone control scheme for wide-speed-range operations [15], [16], [17], [18], [19], [20], [21], [22], [23], [24], [25], [26].

As a startup method for PMSMs, typically, I-f control is used due to its superiority in low speed than that of V/f control. V/f control requires that stator resistance voltage drop and inverter voltage error be compensated to maintain torque production capability in low speed [16], [17]. Another drawback of V/f control is the difficulty of limiting stator current [17], [20], [25]. I-f control does not require the voltage compensation and stator current is limited inherently due to the closed-loop current regulator. Acceptable torque production capability can be provided with a large current magnitude [11]. When the speed is high enough, the control can be switched to FOC. However, as I-f control and FOC are different schemes, a strategy is usually needed for a smooth transition.

Direct transition is reported in [7], however, large transients may occur due to inaccurate parameters. In [8], a pulse-off method is proposed for transition. But additional electric circuit is needed. A method using phase-locked-loop (PLL) is proposed in [14], but details regarding parameter design are not discussed. Methods based on current reduction are more popular, as reported in [9], [10], and [11]. These methods reduce the current of I-f control to move the working point close to the desired one for FOC operation and then perform the switching. However, constant load is assumed during the process of current reduction. As will be demonstrated in Section V, in cases when the load changes during this process, the transition to FOC can fail. A smooth and more stable transition to FOC can be obtained by stabilizing the $i_{\mathrm{d}} = 0$ working point for I-f control of SPMSM drives.

Besides working as a startup method, there is also great interest in scalar control as a standalone scheme for wide-speed-range operations. Conventional open-loop scalar control is poorly damped and inefficient [15], [17], [27]. Many improved versions have been developed over the past 30 plus years [15], [16], [17], [18], [19], [20], [21], [22], [23], [24], [25], [26]. These works augment scalar control by means of feedback, aiming to achieve stable and efficient operation. A feedback loop that adjusts the frequency reference [henceforth called frequency compensation

Manuscript received 16 April 2022; revised 13 July 2022 and 17 December 2022; accepted 10 February 2023. Date of publication 17 February 2023; date of current version 20 April 2023. Recommended for publication by Associate Editor H. Hofmann. *(Corresponding author: Dunzhi Chen.)*

Dunzhi Chen, Kaiyuan Lu, and Dong Wang are with the Department of Energy Technology, Aalborg University, 9220 Aalborg, Denmark (e-mail: dch@et.aau.dk; klu@et.aau.dk; dwa@et.aau.dk).

Marko Hinkkanen is with the Electrical Engineering and Automation, Aalto University, FI-00076 Aalto, Finland (e-mail: marko.hinkkanen@aalto.fi).

Color versions of one or more figures in this article are available at https://doi.org/10.1109/TPEL.2023.3246361.

Digital Object Identifier 10.1109/TPEL.2023.3246361

loop (FCL)], introduced for stabilizing V/f control in [15], has been widely adopted in scalar control, see, e.g., [16], [17], [18], [19], [21], [22], [24], [28], [29]. The FCL increases the damping but does not offer efficient operation as it does not affect the steady-state working point.

To improve efficiency, various methods are used in [15], [16], [19], [21], [22], [23], [24], [26], and [29]. These methods adjust the voltage magnitude of V/f control (or current magnitude of I-f control) to alter the working point for efficient operation. The target is typically maximum torque per ampere (MTPA[1]). However, the search-based methods in [15], [28], and the SI-based method in [26] offer poor dynamic performance as the voltage can only be adjusted slowly. Methods based on reactive power [16], [19], [24], [29] and power factor [21], [22] have been proposed to achieve MTPA. But detailed stability analysis is lacking. In [23], a method that uses estimated d-axis current is proposed to achieve MTPA for V/f control. Yet, stable operation is only demonstrated against ramp load disturbance. For a reliable scalar control scheme, good load disturbance rejection capability is an important feature to have.

To summarize, whether scalar control is used for startup or as a standalone scheme, it is desirable to achieve MTPA. For startup, after a certain speed is reached, it can enable a smooth transition to FOC; whereas for standalone operation, MTPA is needed for energy saving purpose. Due to its superiority, we focus on I-f control in this article and propose an improved version with feedback loops to achieve stable $i_{\mathrm{d}} = 0$ operation for SPMSM drives. Detailed analysis and extensive experimental results verify the effectiveness of the proposed method.

The rest of this article is organized as follows. Section II deals with mathematical modeling. Section III deals with the conventional open-loop I-f control. It is analyzed that the open-loop I-f control is poorly damped and only stable with positive d-axis current. Section IV presents the proposed I-f control with two feedback loops for stable $i_{\mathrm{d}} = 0$ operation. Experimental results are given in Section V. And finally, Section VI concludes this article.

II. SPMSM Model

A. Dynamic Model

The dynamic model of SPMSM on the d^*q^* frame defined in Fig. 1 can be written as

$$\begin{cases} \frac{\mathrm{d}i_{\mathrm{d}^*}}{\mathrm{d}t} = -\frac{R_{\mathrm{s}}}{L} i_{\mathrm{d}^*} + \omega_{\mathrm{e}} i_{\mathrm{q}^*} + \frac{\lambda_{\mathrm{m}}}{L}\omega_{\mathrm{r}}\cos(\delta) + \frac{v_{\mathrm{d}^*}}{L} \\ \frac{\mathrm{d}i_{\mathrm{q}^*}}{\mathrm{d}t} = -\omega_{\mathrm{e}} i_{\mathrm{d}^*} - \frac{R_{\mathrm{s}}}{L} i_{\mathrm{q}^*} - \frac{\lambda_{\mathrm{m}}}{L}\omega_{\mathrm{r}}\sin(\delta) + \frac{v_{\mathrm{q}^*}}{L} \\ \frac{\mathrm{d}\omega_{\mathrm{r}}}{\mathrm{d}t} = \frac{n_{\mathrm{pp}}}{J} T_{\mathrm{e}} - \frac{n_{\mathrm{pp}}}{J} T_{\mathrm{L}} - \frac{1}{J} B_{\mathrm{m}}\omega_{\mathrm{r}} \\ \frac{\mathrm{d}\delta}{\mathrm{d}t} = \omega_{\mathrm{e}} - \omega_{\mathrm{r}} \\ T_{\mathrm{e}} = \frac{3}{2} n_{\mathrm{pp}} \lambda_{\mathrm{m}} \left[i_{\mathrm{q}^*}\sin(\delta) - i_{\mathrm{d}^*}\cos(\delta) \right] \end{cases} \tag{1}$$

where $i_{\mathrm{d}^*}, i_{\mathrm{q}^*}, v_{\mathrm{d}^*}$, and v_{q^*} are d^*- and q^*-axes currents and voltages, n_{pp} is the number of pole pairs, R_{s} is the stator resistance, L is the $d(q)$-axis inductance, B_{m} is the viscous damping coefficient, λ_{m} is the permanent magnet flux linkage,

[1]For SPMSM, MTPA means $i_{\mathrm{d}} = 0$ in this work.

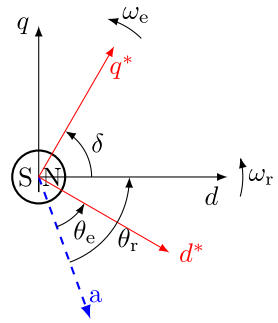

Fig. 1. Reference frame definition. The d^*q^* frame rotates with the reference speed ω_{e}, the dq frame is defined with the d-axis aligned with the rotor north pole and a-axis is the phase a flux axis.

ω_{r} is the rotor speed, ω_{e} is the rotation speed of the d^*q^* reference frame, δ is the angle difference between q^*-axis and d-axis, T_{L} is the load torque and T_{e} is the electromagnetic torque.

For analyzing I-f control, a simplified model that neglects fast current dynamics in (1) will be used. With this simplification, the stator currents are considered equal to the current references ($i_{\mathrm{d}^*} = i_{\mathrm{d}^*}^{\mathrm{ref}} = 0$ and $i_{\mathrm{q}^*} = i_{\mathrm{q}^*}^{\mathrm{ref}}$). The simplified model is given by

$$\begin{cases} \frac{\mathrm{d}\omega_{\mathrm{r}}}{\mathrm{d}t} = \frac{n_{\mathrm{pp}}}{J} T_{\mathrm{e}} - \frac{n_{\mathrm{pp}}}{J} T_{\mathrm{L}} - \frac{B_{\mathrm{m}}}{J}\omega_{\mathrm{r}} \\ \frac{\mathrm{d}\delta}{\mathrm{d}t} = \omega_{\mathrm{e}} - \omega_{\mathrm{r}} \\ T_{\mathrm{e}} = \frac{3}{2} n_{\mathrm{pp}} \lambda_{\mathrm{m}} i_{\mathrm{q}^*}\sin(\delta). \end{cases} \tag{2}$$

B. Small-Signal Model

A small-signal model will be derived in this subsection. Variables with subscript 0 denote steady-state values.

The model in (2) is a nonlinear second-order one with two inputs i_{q^*} and ω_{e} and two states δ and ω_{r}. Linearizing (2) at a steady-state working point gives

$$\begin{cases} \frac{\mathrm{d}\Delta\omega_{\mathrm{r}}}{\mathrm{d}t} = \frac{n_{\mathrm{pp}}}{J}\Delta T_{\mathrm{e}} - \frac{n_{\mathrm{pp}}}{J}\Delta T_{\mathrm{L}} - \frac{B_{\mathrm{m}}}{J}\Delta\omega_{\mathrm{r}} \\ \frac{\mathrm{d}\Delta\delta}{\mathrm{d}t} = \Delta\omega_{\mathrm{e}} - \Delta\omega_{\mathrm{r}} \\ \Delta T_{\mathrm{e}} = K_1\Delta\delta + K_2\Delta i_{\mathrm{q}^*} \end{cases} \tag{3}$$

where $\Delta\omega_{\mathrm{r}}$ denotes small deviation around the steady-state speed, i.e., $\Delta\omega_{\mathrm{r}} = \omega_{\mathrm{r}} - \omega_{\mathrm{r}0}$, and other small-signal terms are defined similarly; the gains K_1 and K_2 can be calculated as

$$\begin{cases} K_1 = \frac{\partial T_{\mathrm{e}}}{\partial\delta}\big|_{\delta_0} = \frac{3}{2} n_{\mathrm{pp}}\lambda_{\mathrm{m}}\cos(\delta_0) i_{\mathrm{q}^*} \\ K_2 = \frac{\partial T_{\mathrm{e}}}{\partial i_{\mathrm{q}^*}}\big|_{\delta_0} = \frac{3}{2} n_{\mathrm{pp}}\lambda_{\mathrm{m}}\sin(\delta_0). \end{cases} \tag{4}$$

Applying the Laplace transform on (3) and rearranging the equations gives

$$\begin{cases} -\Delta\omega_{\mathrm{r}}(s) = \frac{n_{\mathrm{pp}}}{Js + B_{\mathrm{m}}} \left[\Delta T_{\mathrm{L}}(s) - \Delta T_{\mathrm{e}}(s) \right] \\ \Delta\delta(s) = \frac{1}{s} \left[\Delta\omega_{\mathrm{e}}(s) - \Delta\omega_{\mathrm{r}}(s) \right] \\ \Delta T_{\mathrm{e}}(s) = K_1\Delta\delta(s) + K_2\Delta i_{\mathrm{q}^*}(s). \end{cases} \tag{5}$$

The model in (5) can be visualized in Fig. 2. This model will be used for analyzing the conventional open-loop I-f control and the proposed I-f control with feedback loops.

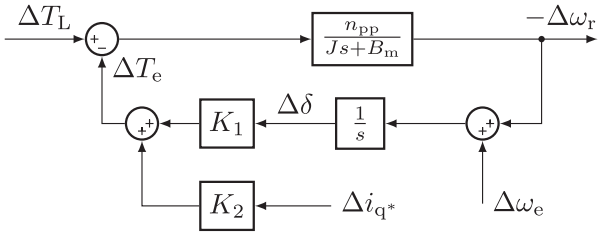

Fig. 2. Small-signal model of SPMSM under I-f control.

III. Conventional Open-Loop I-F Control

A. Basic Principle

Conventional open-loop I-f control is shown in Fig. 3 (without the compensation loops). The I-f control is implemented on the d^*q^* frame (Fig. 1). The angle θ_e for allocating the d^*q^* frame with respect to the a-axis is obtained by integrating the frequency reference ω_e, i.e.,

$$\theta_e = \int \omega_e \mathrm{d}t. \tag{6}$$

As shown in Fig. 3, the current vector is regulated to be on the q^*-axis with PI controllers and the current references are

$$i_{d^*}^{\mathrm{ref}} = 0,\ i_{q^*}^{\mathrm{ref}} = I_0 \tag{7}$$

where I_0 is generally chosen to be a large value (e.g., the rated value) for sufficient torque generation capability [9], [11].

For startup, the initial value of θ_e is set to $-\pi/2$ and the current vector will be aligned with the d-axis, as shown in Fig. 4(a). In this stage, there will be no torque output. Then, as θ_e increases through (6), the current vector will rotate counterclockwise from the d-axis [see Fig. 4(b)] and electromagnetic torque will increase according to

$$T_e = \frac{3}{2} n_{pp} \lambda_m I_0 \sin(\delta). \tag{8}$$

When T_e is greater than the load torque, the machine will start to rotate.

B. Open-Loop I-F Control Characteristics

The steady-state working point of an SPMSM under the conventional open-loop I-f control can be obtained by solving $\mathrm{d}/\mathrm{d}t = 0$ in (2) as

$$\omega_{r0} = \omega_{e0} \tag{9}$$

$$\delta_0 = \arcsin\left(\frac{T_{L0} + \frac{B_m \omega_{r0}}{n_{pp}}}{\frac{3}{2} n_{pp} \lambda_m I_0}\right). \tag{10}$$

Since there is no compensation loop for the conventional open-loop I-f control, the corresponding model can be obtained by letting $\Delta i_{q^*} = 0, \Delta\omega_e = 0$ in Fig. 2. The transfer function from the load torque to the rotor speed can be obtained as

$$\frac{-\Delta\omega_r(s)}{\Delta T_L(s)} = \frac{n_{pp} s}{Js^2 + B_m s + K_1 n_{pp}}. \tag{11}$$

The poles for (11) are

$$p_{1,2} = -\frac{B_m}{2J} \pm \sqrt{\frac{B_m^2}{4J^2} - \frac{K_1 n_{pp}}{J}}. \tag{12}$$

According to (12), one can see the following.

1) The system is stable when $K_1 > 0$, which according to (4) requires that $\delta_0 \in (0, \pi/2)$. This means open-loop I-f control can only work stably with positive d-axis current.
2) Even when stable, the system is poorly damped. The damping is only provided by the viscous damping coefficient, which is usually small. Without the viscous damping coefficient ($B_m = 0$), it is clear from (12) that the poles will be on the imaginary axis and the system is only marginally stable.

IV. Proposed I-F Control

Conventional open-loop I-f control is poorly damped and only stable with positive d-axis current. To achieve stable $i_d = 0$ operation, two feedback loops (FCL and CCL in Fig. 3) are used in the proposed I-f control.

A. The FCL

The FCL (in Fig. 3) is a widely adopted solution for damping of scalar controlled PMSM drives. The FCL can be implemented based on [17]

$$p_e = \frac{3}{2}(v_\alpha^* i_\alpha + v_\beta^* i_\beta) \tag{13}$$

$$\Delta p_e = \frac{\tau s}{\tau s + 1} p_e \tag{14}$$

$$\Delta\omega_e = -K_p \Delta p_e \tag{15}$$

where v_α^*, v_β^*, i_α, i_β are the $\alpha\beta$-axes voltage commands and currents, τ is the time constant of the first-order high-pass filter and K_p is a proportional gain. Basically, the FCL adjusts the frequency reference using the perturbation component of active power. The active power is calculated by (13). Then, its perturbation component obtained by (14) is used to generate the frequency compensation signal in (15), which is added to the original frequency reference as shown in Fig. 3. For more details on the FCL, refer to [17].

In what follows, we will show that the FCL can provide extra damping for I-f control, but it does not offer stable $i_d = 0$ operation. Linearizing the power balance equation around a steady-state point, it can be found that the perturbation component of active power is related to rotor speed variation as [17]

$$\Delta p_e = \frac{J\omega_{r0}}{n_{pp}^2} \frac{\mathrm{d}\Delta\omega_r}{\mathrm{d}t} + \frac{2B_m\omega_{r0}}{n_{pp}^2}\Delta\omega_r + \frac{T_{L0}}{n_{pp}}\Delta\omega_r. \tag{16}$$

Based on (15) and (16), the frequency compensation signal can be obtained as

$$\begin{aligned}\Delta\omega_e &= -K_p \Delta p_e \\ &= -K_p\left(\frac{J\omega_{r0}}{n_{pp}^2}\frac{\mathrm{d}\Delta\omega_r}{\mathrm{d}t} + \frac{2B_m\omega_{r0}}{n_{pp}^2}\Delta\omega_r + \frac{T_{L0}}{n_{pp}}\Delta\omega_r\right).\end{aligned} \tag{17}$$

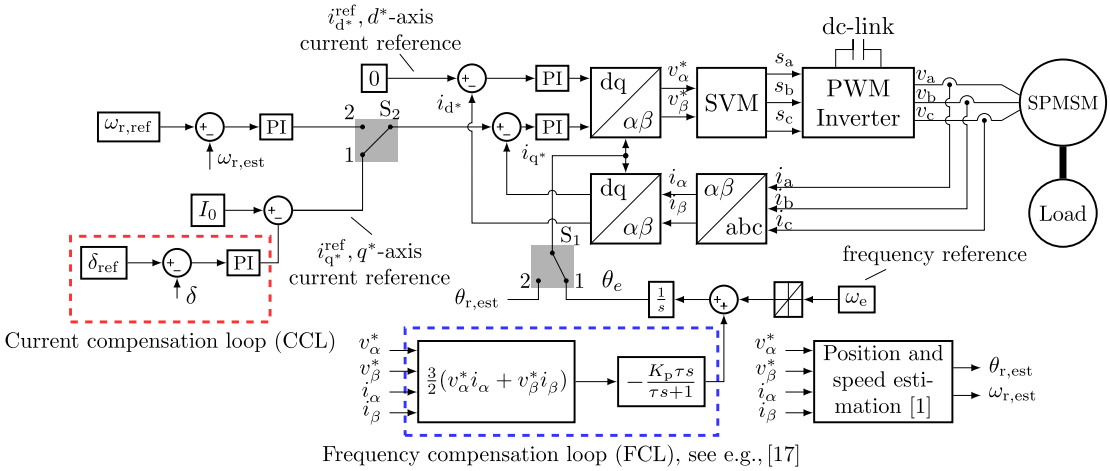

Fig. 3. I-f control for SPMSM drives. The compensation loops (FCL and CCL) are not used for conventional open-loop I-f control and will be discussed in Section IV. As I-f control is usually used for startup, switching to FOC is also included here. The two switches (S_1 and S_2) are connected to terminal 1 for the I-f control and 2 for sensorless FOC.

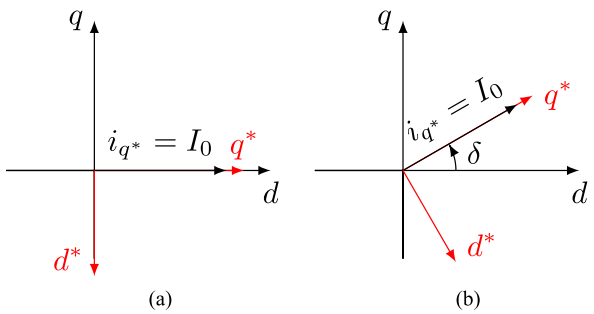

Fig. 4. Basic principle for open-loop I-f control for startup. (a) Initially, the current vector is aligned with the d-axis, no torque output. (b) Current vector rotates counterclockwise away from the d-axis and torque is generated.

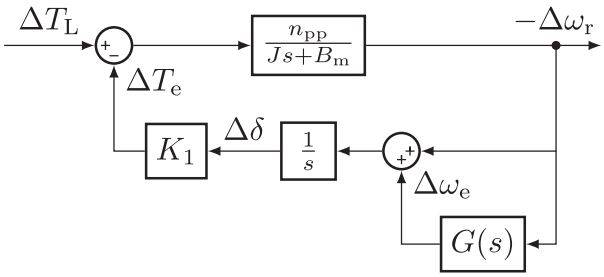

Fig. 5. Small-signal model of SPMSM under I-f control with the FCL.

Letting $\Delta i_{q^*} = 0$ and $\Delta\omega_e$ be (17) in Fig. 2, the model for SPMSM under I-f control with the FCL can be obtained as shown in Fig. 5, where

$$G(s) = \frac{\Delta\omega_e(s)}{-\Delta\omega_r(s)} = \frac{K_p J\omega_{r0}}{n_{pp}^2}s + \frac{2K_p B_m\omega_{r0}}{n_{pp}^2} + \frac{K_p T_{L0}}{n_{pp}}. \tag{18}$$

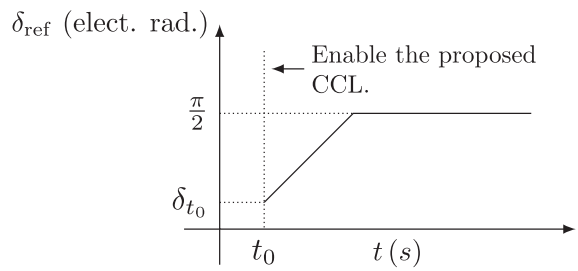

Fig. 6. Current vector position reference profile for the proposed CCL. The CCL is enabled at t_0 and the initial value for angle reference δ_{ref} is set to be δ_{t0} and then slowly increased to $\pi/2$.

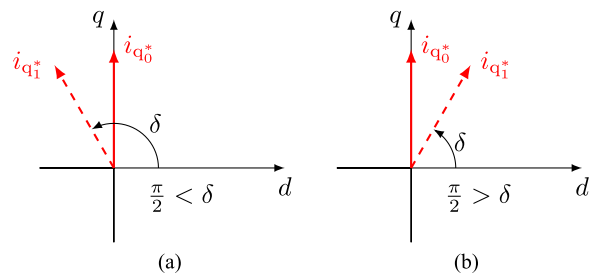

Fig. 7. $i_d = 0$ operation point of SPMSM under the I-f control perturbed by load disturbance. (a) Positive load disturbance, machine slows down, current vector moves from q-axis to the second quadrant. (b) Negative load disturbance, machine speeds up, current vector moves to the first quadrant.

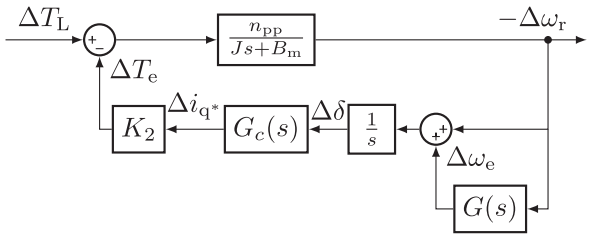

Fig. 8. Small-signal model of SPMSM under I-f control with the FCL and the proposed CCL.

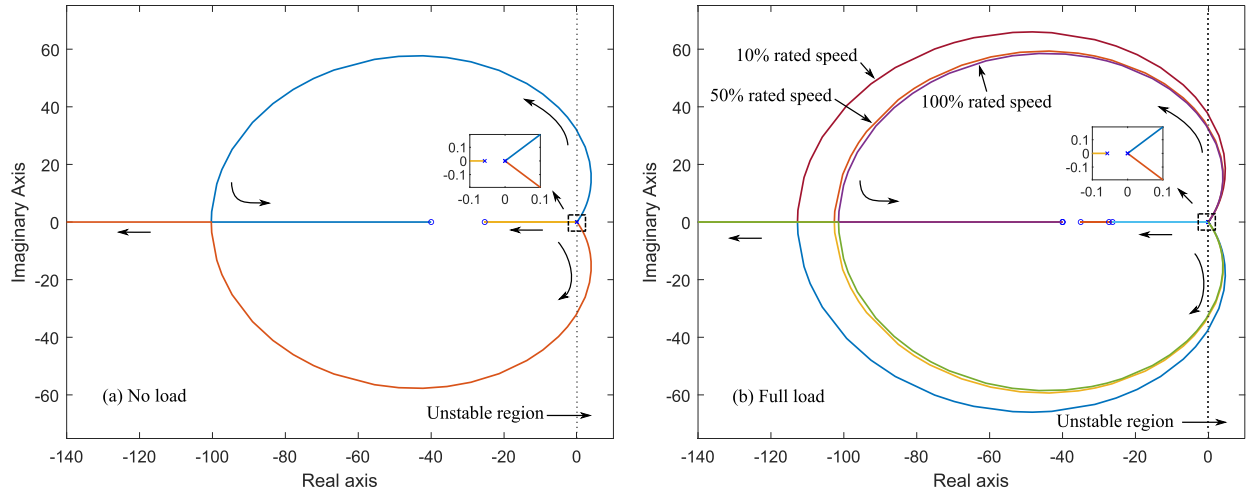

Fig. 9. Loci of closed-loop poles for the model in Fig. 8 as $K_{\rm pc}$ goes from 0 to ∞ under different speed and load conditions. (a) No load. (b) Full load. For each load condition, 10%, 50%, and 100% rated speed are included.

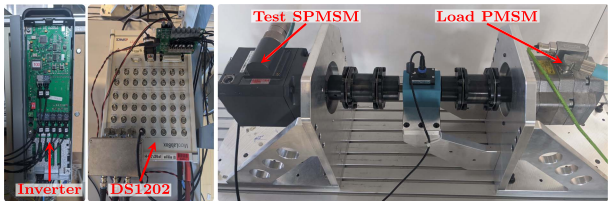

Fig. 10. Experimental setup.

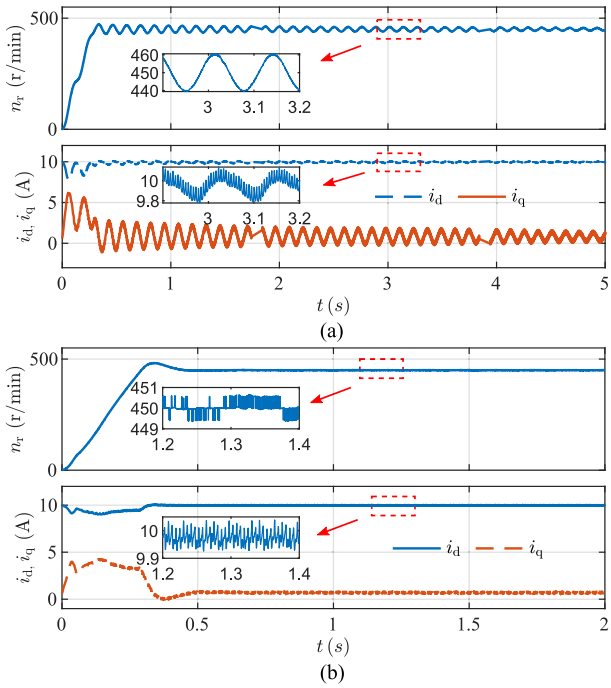

Fig. 11. Performance of I-f control. (a) Conventional open-loop I-f control, poor damping. (b) I-f control with the FCL, damping increased.

The closed-loop transfer function for the system in Fig. 5 can be obtained as

$$\frac{-\Delta\omega_{\rm r}(s)}{\Delta T_{\rm L}(s)}=\frac{n_{\rm pp}s}{Js^2+(B_{\rm m}+\frac{\omega_{\rm r0}K_{\rm p}K_1J}{n_{\rm pp}})s+n_{\rm pp}K_1(1+K_{\rm p}C)} \tag{19}$$

where $C=2B_{\rm m}\omega_{\rm r0}/n_{\rm pp}^2+T_{\rm L0}/n_{\rm pp}$. The closed-loop poles are

$$p_{1,2}=-\frac{\omega_{\rm r0}K_{\rm p}K_1}{2n_{\rm pp}}-\frac{B_{\rm m}}{2J} \pm\sqrt{\left(\frac{\omega_{\rm r0}K_{\rm p}K_1}{2n_{\rm pp}}+\frac{B_{\rm m}}{2J}\right)^2-\frac{n_{\rm pp}K_1(1+K_{\rm p}C)}{J}}. \tag{20}$$

A comparison between (12) and (20) shows that the FCL can move the poles further to the left of the complex plane, which indicates faster convergence. However, $i_{\rm d}=0$ operation is unstable because at this working point, we have $\delta_0=\pi/2$ and therefore, $K_1=0$. From Fig. 5, one can see that when $K_1=0$, $\Delta\omega_{\rm e}$ does not affect $\Delta T_{\rm e}$ anymore. This clearly indicates that the $i_{\rm d}=0$ point is unstable.

B. Current Compensation Loop

The FCL can increase damping but does not enable stable $i_{\rm d}=0$ operation. To achieve stable $i_{\rm d}=0$ operation, an additional feedback loop (CCL in Fig. 3) that adjusts the q^*-axis current is proposed. Using the CCL, the current command for the I-f control is modified to

$$i_{\rm q^*}=I_0-K_{\rm pc}(\delta_{\rm ref}-\delta)-K_{\rm ic}\int(\delta_{\rm ref}-\delta){\rm d}t \tag{21}$$

where $K_{\rm pc}$ and $K_{\rm ic}$ are the PI controller parameters, δ is current vector position with respect to the d-axis (see Fig. 1) and $\delta_{\rm ref}$ is the current vector position reference. The angle δ can be obtained as

$$\delta\approx\theta_{\rm e}+\frac{\pi}{2}-\theta_{\rm r,est} \tag{22}$$

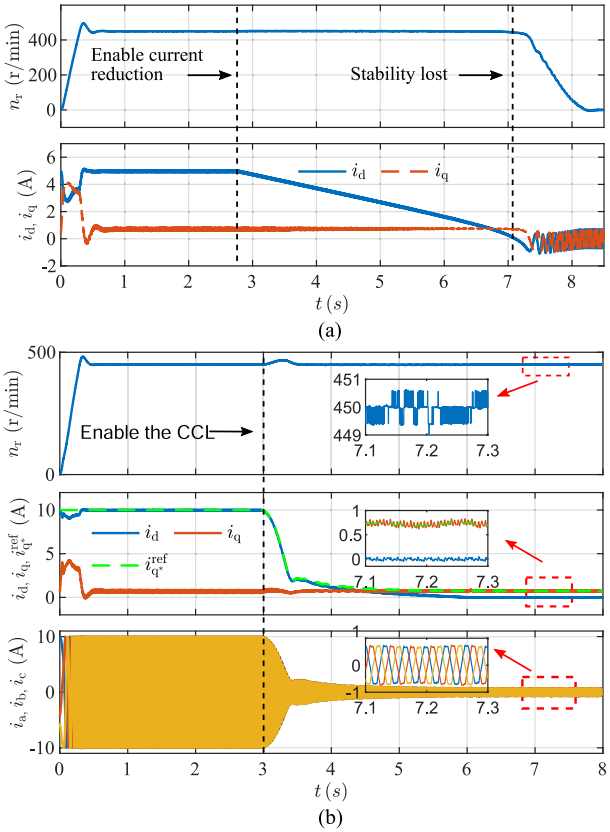

Fig. 12. Stability of $i_d = 0$ operation for I-f control. (a) I-f control with the FCL, $i_d = 0$ unstable. (b) I-f control with the FCL and the proposed CCL enabled at $t = 3$ s, $i_d = 0$ stabilized.

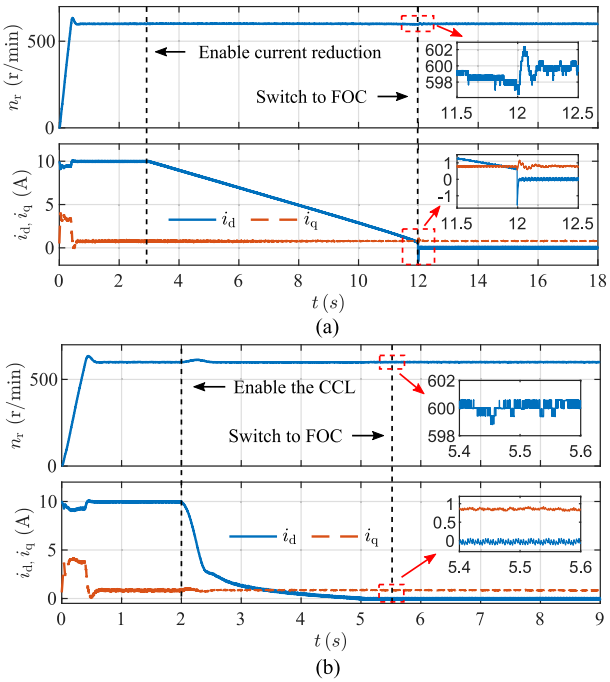

Fig. 13. Transition to sensorless FOC comparison, constant load. (a) Current reduction method in [9], [11], and [12]. (b) Proposed CCL.

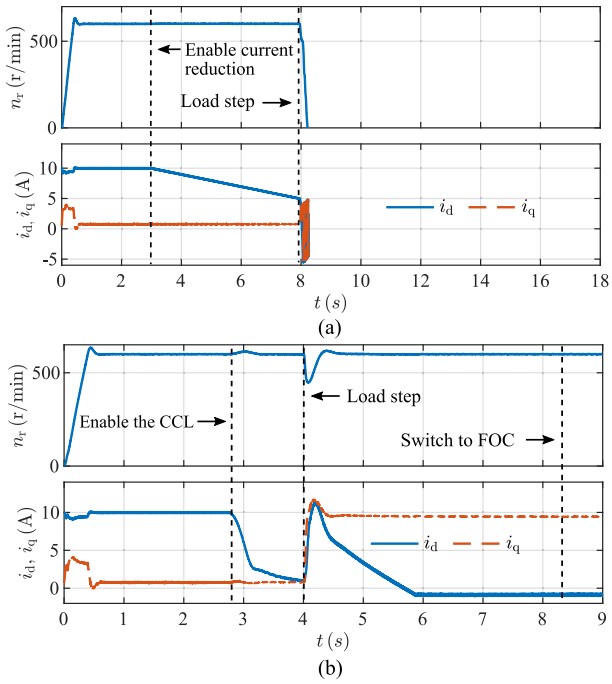

Fig. 14. Transition to sensorless FOC comparison, with load disturbance in the transition process. (a) Current reduction method in [9], [11], and [12] (b) Proposed CCL.

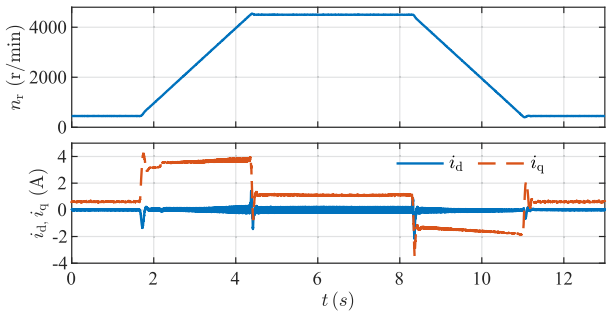

Fig. 15. I-f control with the FCL and the proposed CCL, speed ramp-up from 450 to 4500 r/min and down to 450 r/min under no load.

where $\theta_{r,est}$ is the estimated rotor position from the back EMF method [1].

As the estimated rotor position is used, the CCL is only enabled after the machine reaches a certain speed. The reference profile of δ_{ref} is shown in Fig. 6. To avoid large transients, the initial value of δ_{ref} is set as the value of δ the instant when enabling the loop (denoted as δ_{t0}). Then, δ_{ref} is increased from δ_{t_0} to $\pi/2$ to move the current vector to the q-axis, i.e., achieving $i_d = 0$ operation.

With the CCL, the steady-state working point becomes $i_d = 0$. The basic idea of how this working point can be stabilized is explained next. Consider Fig. 7, where initially the current vector is on the q-axis ($i_{q_0^*}$). When torque increases [see Fig. 7(a)], the machine slows down, and the current vector will move to the second quadrant (from $i_{q_0^*}$ to $i_{q_1^*}$), resulting in $\delta > \pi/2$ and consequently an increase of i_{q^*} according to (21). This will

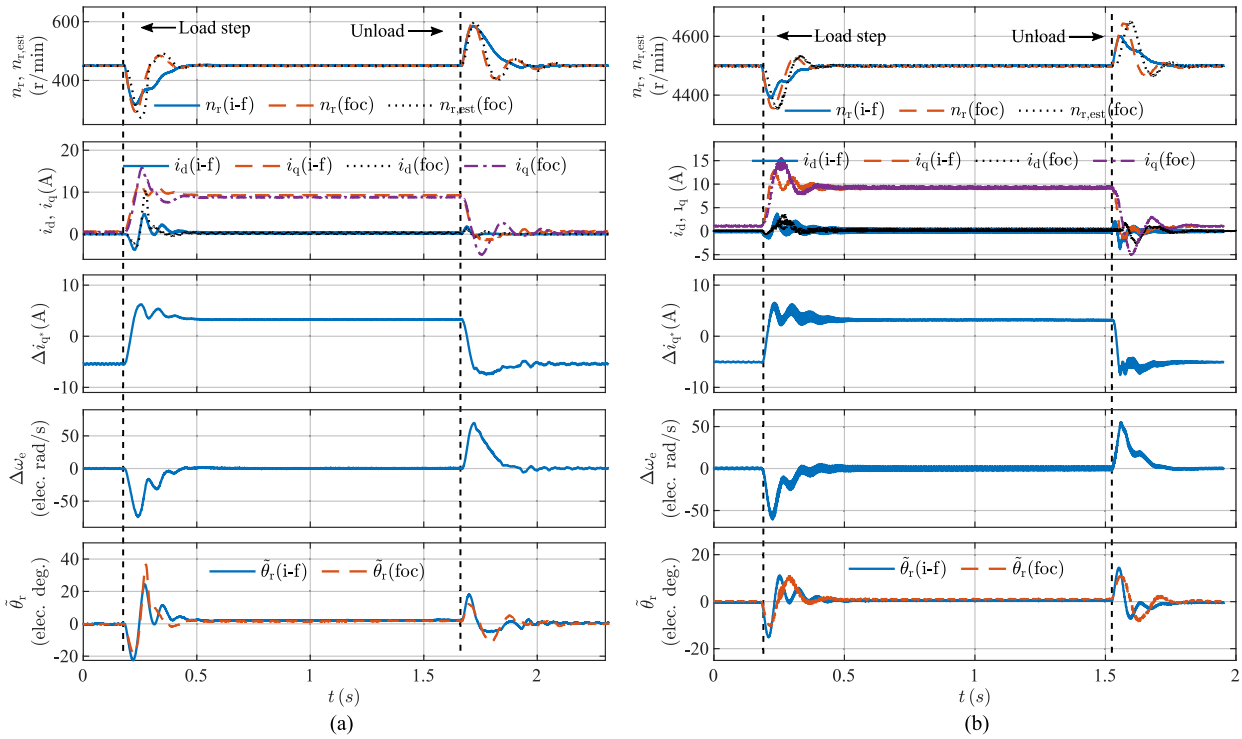

Fig. 16. Load rejection comparison between the I-f control and sensorless FOC, 100% rated load step applied and then released. (a) 450 r/min. (b) 4500 r/min.

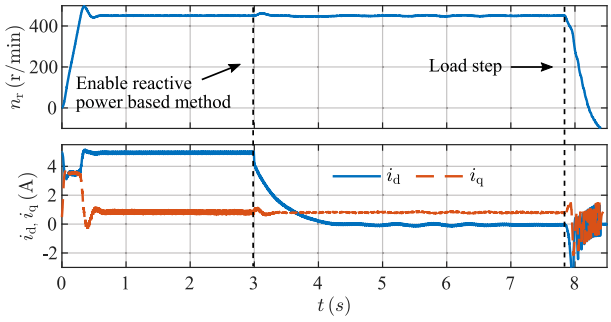

Fig. 17. I-f control using reactive power-based method for adjusting the current magnitude to achieve $i_d = 0$ operation. Instability occurs with a 2 N·m (34% rated) load step disturbance.

increase the electromagnetic torque to balance the increased load torque. The PI controller used in the loop will continue to regulate the current magnitude until $\delta = \pi/2$. Similarly, when the load torque reduces [see Fig. 7(b)], the PI controller will reduce the current magnitude until $\delta = \pi/2$.

C. Stability Analysis

For the I-f control with the FCL and the CCL, in steady state, we have $\delta_0 = \pi/2$. Linearizing (21) at $\delta_0 = \pi/2$, we have

$$\Delta i_{q^*} = K_{pc}\Delta\delta + K_{ic}\int \Delta\delta \mathrm{d}t. \tag{23}$$

By inserting the current magnitude compensation term Δi_{q^*} given in (23) and the frequency compensation term $\Delta\omega_e$ given in (17) to the small-signal model in Fig. 2, the model for SPMSM under the I-f control with FCL and the proposed CCL can be obtained as shown in Fig. 8, where $G_c(s)$ is the PI controller transfer function

$$G_c(s) = \frac{K_{pc}\left(s + \frac{K_{ic}}{K_{pc}}\right)}{s}. \tag{24}$$

The model in Fig. 8 contains three control parameters that need to be tuned. The tuning of K_p for the FCL in $G(s)$ is well-documented, see, e.g., [17]. We use root-locus to show how K_{pc} and K_{ic} in $G_c(s)$ can be tuned for stable operation. For this, the open-loop transfer function for the system in Fig. 8 is obtained as

$$G_{ol}(s) = \frac{\Delta T_e(s)}{\Delta T_L(s)} = G_c(s)G_p(s) \tag{25}$$

where

$$G_p(s) = \frac{K_2 n_{pp}}{Js^2 + B_m s}\left[1 + G(s)\right]. \tag{26}$$

According to the locations of zeros and poles in $G_p(s)$, the zero in $G_c(s)$ (i.e., K_{ic}/K_{pc}) is assigned first. Then the location of closed-loop poles is a function of K_{pc} alone, and can be tuned using the root-locus. For example, with the zero of $G_c(s)$ assigned at -40, the root-locus (K_{pc} increases from zero to infinity) for the system under different speed and load conditions is shown in Fig. 9. It can be seen when K_{pc} increases, the closed-loop poles first move to the right and then to the left side of the complex plane, which indicates with large enough K_{pc}, the system can be stabilized.

TABLE I
DATA OF THE 2.7-KW EIGHT-POLE SPMSM

Rated values		*Parameters*	
Current (RMS)	7.4 A	Stator resistance R_s	1.2 Ω
Torque	5.8 N·m	$d(q)$-axis inductance L	5.5 mH
Frequency	300 Hz	Flux linkage by PM λ_m	0.1213 Wb-t
Speed	4500 r/min	Total inertia J	0.0125 kg·m^2

V. EXPERIMENTAL RESULTS

Experiments are carried out on a setup shown in Fig. 10, which consists of a test SPMSM (parameters in Table I), a load PMSM, a dSPACE 1202 (DS1202) and a Danfoss FC302 inverter. A 4096-line encoder is used to obtain the rotor position and speed for verification only. The pulse width modulation (PWM) switching frequency and the sampling frequency is 8 kHz. Experimental data are recorded in ControlDesk and exported to MATLAB for plotting the figures.

The main control parameters used are: the PI controllers for regulating d^*q^*-axes currents are $K_{\mathrm{p,cur}} = 10.6$ and $K_{\mathrm{i,cur}} = 1921$; for the FCL, the time constant $\tau = 0.0637$ and $K_{\mathrm{p}} = 40/\omega_{\mathrm{e0}}(\omega_{\mathrm{e0}} \neq 0)$; for the proposed CCL, $K_{\mathrm{pc}} = 100$ and $K_{\mathrm{ic}} = 4000$. In all the results presented in this section, the machine is first aligned to a known position by applying a constant voltage vector on the α-axis. All dq-axes mentioned in experimental results mean actual dq-axes based on the encoder.

A. Open-Loop and the Proposed I-F Control

Fig. 11(a) shows performance of the conventional open-loop I-f control. The q^*-axis current reference for I-f control is generally chosen to be a large value for reliable startup [9], [11] and $I_0 = 10$ A (close to the rated current) is used here. In Fig. 11(a), the speed and dq-axes currents oscillate and converge slowly. This is due to the poor damping as analyzed in Section III.

Fig. 11(b) shows performance of I-f control with the FCL. It can be seen that the speed and currents in Fig. 11(b) converge much faster as compared with Fig. 11(a). This confirms the damping effect of the FCL. However, the FCL does not affect the steady-state working point. As can be seen in both cases [see Fig. 11(a) and (b)], there exists a large steady-state d-axis current, which is not desired.

The steady-state d-axis current can be reduced by using a smaller q^*-axis current reference. However, $i_{\mathrm{d}} = 0$ operation is unstable for I-f control with the FCL alone. This is demonstrated in Fig. 12(a), where the q^*-axis current reference is reduced slowly to move the working point to $i_{\mathrm{d}} = 0$. When $i_{\mathrm{d}} > 0$, stable operation can be maintained, however, once $i_{\mathrm{d}} = 0$, the stability is lost.

The CCL is proposed to achieve stable $i_{\mathrm{d}} = 0$ operation for the I-f control. As shown in Fig. 12(b), when the proposed CCL is enabled at $t = 3$ s, the d-axis current reduces to zero and this desired operation condition can be maintained. This confirms that the $i_{\mathrm{d}} = 0$ working point is stabilized.

B. As a Startup Method

I-f control is usually used for startup and the control is switched to sensorless FOC when the speed is high enough. The proposed CCL can be used to obtain a smooth transition and its performance is compared with a commonly used current reduction method [9], [11], [12] in Fig. 13. For the results shown in Fig. 13, I-f control with the FCL is used to start the machine to a steady speed. Current reduction is used to move the working point close to $i_{\mathrm{d}} = 0$ before switching to FOC in Fig. 13(a), whereas the control is switched to FOC after $i_{\mathrm{d}} = 0$ is achieved by the proposed CCL in Fig. 13(b). As can be seen, the current reduction method produces visible transients when switching to FOC, while the proposed method offers a smoother transition, since the desired $i_{\mathrm{d}} = 0$ operation is already achieved before switching to FOC.

More importantly, the transition process using the proposed CCL is more stable than the current reduction method. The current reduction method assumes constant load, however, as demonstrated in Fig. 14(a), when a 3 N·m load disturbance is applied during current reduction process, transition to FOC failed. Whereas in Fig. 14(b), a 5.8 N·m load step disturbance is rejected by the proposed CCL and after steady state is reached, the control is switched to FOC successfully and smoothly.

C. As a Standalone Scheme

The proposed I-f control may also be used as a standalone scheme as stable $i_{\mathrm{d}} = 0$ operation can now be maintained in a wide speed range with good load disturbance rejection capability. Fig. 15 shows the performance from 450 to 4500 r/min and down to 450 r/min using the I-f control with the FCL and the CCL under no load condition.

Load rejection capability of the proposed method is tested and compared with a classical back EMF-based sensorless FOC in Fig. 16. The same rotor position estimator [1] applied in the I-f control is used for the sensorless FOC. Load step of 5.8 N·m (100% rated) is applied and then released for both schemes at 450 and 4500 r/min, respectively. The I-f control can well reject rated load step and maintain stable $i_{\mathrm{d}} = 0$ operation with comparable transient and steady-state performance with the FOC.

The reactive power-based method documented in detail in [16] and [29] is implemented for comparison. The result is shown in Fig. 17. When the reactive power-based loop is enabled at $t = 3$ s, the d-axis current reduces to zero. However, when a 2 N·m (34% rated) step load disturbance is applied, the stability is lost. The proposed I-f control in this article has shown much better performance with respect to load disturbance rejection than the reactive power-based method.

VI. CONCLUSION

The conventional open-loop I-f control for SPMSM drives is poorly damped and only stable with positive d-axis current. The FCL can provide extra damping, but it does not offer $i_{\mathrm{d}} = 0$ operation. An I-f control with the FCL and a new CCL is proposed in this work for stabilization of $i_{\mathrm{d}} = 0$ operation for SPMSM

drives. The proposed I-f control can be used as a startup scheme with a smooth and more stable transition to FOC than existing transition methods based on current reduction. In addition, the proposed method can also be used as a standalone scheme for wide-speed-range operations, since it can work stably at $i_{\mathrm{d}} = 0$ operation point from 10% to 100% rated speed with 100% load step rejection capability. Stability analysis, various transient, and steady-steady experimental results and comparisons with existing methods have shown promising results.

REFERENCES

[1] I. Boldea, M. C. Paicu, and G. Andreescu, "Active flux concept for motion-sensorless unified ac drives," *IEEE Trans. Power Electron.*, vol. 23, no. 5, pp. 2612–2618, Sep. 2008.

[2] D. Wang, K. Lu, and P. O. Rasmussen, "Improved closed-loop flux observer based sensorless control against system oscillation for synchronous reluctance machine drives," *IEEE Trans. Power Electron.*, vol. 34, no. 5, pp. 4593–4602, May 2019.

[3] H. Kim, J. Son, and J. Lee, "A high-speed sliding-mode observer for the sensorless speed control of a PMSM," *IEEE Trans. Ind. Electron.*, vol. 58, no. 9, pp. 4069–4077, Sep. 2011.

[4] G. Wang, M. Valla, and J. Solsona, "Position sensorless permanent magnet synchronous machine drives–a review," *IEEE Trans. Ind. Electron.*, vol. 67, no. 7, pp. 5830–5842, Jul. 2020.

[5] G. Wang, R. Yang, and D. Xu, "DSP-based control of sensorless IPMSM drives for wide-speed-range operation," *IEEE Trans. Ind. Electron.*, vol. 60, no. 2, pp. 720–727, Feb. 2013.

[6] S.-C. Yang and Y.-L. Hsu, "Full speed region sensorless drive of permanent-magnet machine combining saliency-based and back-EMF-based drive," *IEEE Trans. Ind. Electron.*, vol. 64, no. 2, pp. 1092–1101, Feb. 2017.

[7] C. L. Baratieri and H. Pinheiro, "I-F starting method for smooth and fast transition to sensorless field oriented control of bldc motors," *Eletrônica de Potência*, vol. 19, no. 3, pp. 268–276, Jul. 2018.

[8] S. V. Nair, K. Hatua, N. Durga Prasad, and D. Kishore Reddy, "Quick and seamless transition method for I-F to sensorless vector control changeover and on-the-fly start of PMSM drives," *IET Electric Power Appl.*, vol. 14, no. 11, pp. 2231–2242, Nov. 2020.

[9] Z. Wang, K. Lu, and F. Blaabjerg, "A simple startup strategy based on current regulation for back-EMF-based sensorless control of PMSM," *IEEE Trans. Power Electron.*, vol. 27, no. 8, pp. 3817–3825, Feb. 2012.

[10] H. Li, X. Zhang, S. Liu, and C. Xu, "Hybrid sensorless control based on I/F and sliding mode observer using current nonlinear regulation for PMSM drives," in *Proc. 22nd Int. Conf. Elect. Mach. Syst.*, 2019, pp. 1–5.

[11] Q. Tang, D. Chen, and X. He, "Integration of improved flux linkage observer and I–F starting method for wide-speed-range sensorless SPMSM drives," *IEEE Trans. Power Electron.*, vol. 35, no. 8, pp. 8374–8383, Aug. 2020.

[12] J. Xing, Z. Qin, C. Lin, and X. Jiang, "Research on startup process for sensorless control of PMSMs based on I-F method combined with an adaptive compensator," *IEEE Access*, vol. 8, pp. 70812–70821, 2020.

[13] S. V. Nair, K. Hatua, N. V. P. R. D. Prasad, and D. K. Reddy, "A quick i–f starting of PMSM drive with pole slipping prevention and reduced speed oscillations," *IEEE Trans. Ind. Electron.*, vol. 68, no. 8, pp. 6650–6661, Aug. 2021.

[14] Q. Li, X. Wang, J. Jiang, Q. Zhang, and Q. Tong, "Sensorless control for surface mounted pm machine with a high inertial load," *CES Trans. Eletcr. Mach. Syst.*, vol. 2, no. 1, pp. 116–122, Mar. 2018.

[15] R. Colby and D. Novotny, "An efficiency-optimizing permanent-magnet synchronous motor drive," *IEEE Trans. Ind. Appl.*, vol. 24, no. 3, pp. 462–469, May/Jun. 1988.

[16] J. I. Itoh, N. Nomura, and H. Ohsawa, "A comparison between V/F control and position-sensorless vector control for the permanent magnet synchronous motor," in *Proc. Power Convers. Conf.*, 2002, pp. 1310–1315.

[17] P. D. Chandana Perera, F. Blaabjerg, J. K. Pedersen, and P. Thøgersen, "A sensorless, stable V/f control method for permanent-magnet synchronous motor drives," *IEEE Trans. Ind. Appl.*, vol. 39, no. 3, pp. 783–791, May 2003.

[18] F. Haichao, S. Boyang, and G. Lizhen, "A closed-loop I/f vector control for permanent magnet synchronous motor," in *Proc. 9th Int. Conf. Model. Identification Control*, 2018, pp. 965–969.

[19] J.-I. Itoh, Y. Nakajima, and G. T. Chiang, "Maximum torque per ampere and maximum efficiency control methods based on V/f control for IPM synchronous motors," *IEEJ J. Ind. Appl.*, vol. 3, no. 2, pp. 112–120, Feb. 2014.

[20] R. Ancuti, I. Boldea, and G.-D. Andreescu, "Sensorless V/f control of high-speed surface permanent magnet synchronous motor drives with two novel stabilising loops for fast dynamics and robustness," *IET Elect. Power Appl.*, vol. 4, no. 3, pp. 149–157, Feb. 2010.

[21] G.-D. Andreescu, C.-E. Coman, S.-C. Agarlita, and I. Boldea, "Stable V/f control system with controlled power factor angle for permanent magnet synchronous motor drives," *IET Elect. Power Appl.*, vol. 7, no. 4, pp. 278–286, Jul. 2013.

[22] A. Consoli, G. Scelba, G. Scarcella, and M. Cacciato, "An effective energy-saving scalar control for industrial IPMSM drives," *IEEE Trans. Ind. Electron.*, vol. 60, no. 9, pp. 3658–3669, Sep. 2013.

[23] Z. Tang, X. Li, S. Dusmez, and B. Akin, "A new V/f-based sensorless MTPA control for IPMSM drives," *IEEE Trans. Power Electron.*, vol. 31, no. 6, pp. 4400–4415, Jun. 2016.

[24] H. Shen and C. Zhang, "A new efficient sensorless I/f control method for IPMSM drives," in *Proc. IEEE Int. Symp. Ind. Electron.*, 2017, pp. 209–213.

[25] A. S. Isfanuti, M. C. Paicu, L. N. Tutelea, T. Staudt, and I. Boldea, "V/f with stabilizing loops versus FOC of Spoke-PM rotor SM drive: Control with experiments," in *Proc. IEEE Int. Conf. Power Electron. Motion Control*, 2018, pp. 629–636.

[26] K. Lee and Y. Han, "Mtpa control strategy based on signal injection for V/f scalar-controlled surface permanent magnet synchronous machine drives," *IEEE Access*, vol. 8, pp. 96036–96044, 2020.

[27] D. Chen, K. Lu, D. Wang, and M. Hinkkanen, "A small-signal stability study for open-loop I-f control of permanent magnet synchronous machine drives," in *Proc. 4th Int. Conf. Energy, Elect. Power Eng.*, 2021, pp. 405–409.

[28] J. I. Itoh, T. Toi, and M. Kato, "Maximum torque per ampere control using hill climbing method without motor parameters based on V/f control," in *18th Eur. Conf. Power Electron. Appl.*, 2016, pp. 1–10.

[29] D. Chen, K. Lu, and D. Wang, "An I-f startup method with compensation loops for PMSM with smooth transition," *IEEJ J. Ind. Appl.*, vol. 9, no. 3, pp. 263–270, Jul. 2020.

Dunzhi Chen (Student Member, IEEE) received the B.S. degree from the Jiangsu University of Science and Technology, Zhangjiagang, China, in 2015, and the M.S. degree from Shanghai Maritime University, Shanghai, China, in 2017, all in electrical engineering. He is currently working toward the Ph.D. degree in electrical engineering with the Aalborg University, Aalborg, Denmark.

His research interest includes control of permanent magnet synchronous machine drives.

Kaiyuan Lu (Member, IEEE) received the B.S. and M.S. degrees from Zhejiang University, Zhejiang, China, in 1997 and 2000 respectively, and the Ph.D. degree from Aalborg University, Denmark, in 2005, all in electrical engineering.

In 2005, he became an Assistance Professor with the Department of Energy Technology, Aalborg University, where he has been an Associate Professor since 2008. His research interests include design of permanent magnet machines, finite element method analysis, and control of permanent magnet machines.

Dong Wang (Member, IEEE) received the B.S. degree from Zhejiang University, Zhejiang, China, in 2004, and the M.S. and Ph.D. degrees from Aalborg University, Denmark, in 2006 and 2016, respectively, all in electrical engineering.

From 2006 to 2012, he was with Grundfos R&D China, Suzhou, China, as a Senior Motor Engineer, working on the design and analysis of the permanent magnet machine and devices. In 2017, he became an Assistant Professor with the Department of Energy Technology, Aalborg University, where he has been an Associate Professor since 2021. His research interests include design and control of electrical machine system, as well as slim dc-link drive.

Marko Hinkkanen (Fellow, IEEE) received the M.Sc.(Eng.) and D.Sc.(Tech.) degrees in electrical engineering from the Helsinki University of Technology, Espoo, Finland, in 2000 and 2004, respectively.

He is currently an Associate Professor (tenured) with the School of Electrical Engineering, Aalto University, Espoo, Finland. His research interests include control systems, electric drives, and power converters.

Dr. Hinkkanen was the recipient of six paper awards, including the 2016 International Conference on Electrical Machines (ICEM) Brian J. Chalmers Best Paper Award, and the 2016 and 2018 IEEE Industry Applications Society Industrial Drives Committee Best Paper Awards. He was the corecipient of the 2020 SEMIKRON Innovation Award. He was the General Cochair of the 2018 IEEE 9th International Symposium on Sensorless Control for Electrical Drives (SLED). He is an Associate Editor of IEEE TRANSACTIONS ON ENERGY CONVERSION and the *IET Electric Power Applications*.